Published in final edited form as:
*J Phys Chem B*. 2013 July 25; 117(29): 8758–8769. doi:10.1021/jp402839r.

# Comparative Computer Simulation Study of Cholesterol in Hydrated Unary and Binary Lipid Bilayers and in an Anhydrous Crystal

**Elzbieta Plesnar**[a], **Witold K. Subczynski**[b], and **Marta Pasenkiewicz-Gierula**[a,*]

[a]Department of Computational Biophysics and Bioinformatics, Faculty of Biochemistry, Biophysics and Biotechnology, Jagiellonian University, Krakow, Poland [b]Department of Biophysics, Medical College of Wisconsin, Milwaukee, Wisconsin, USA

## Abstract

Models created with molecular dynamics simulations are used to compare the organization and dynamics of cholesterol (Chol) molecules in three different environments: (1) a hydrated pure Chol bilayer that models the Chol bilayer domain, which is a pure Chol domain embedded in the bulk membrane; (2) a 2-palmitoyl-3-oleoyl-*D*-glycerol-1-phosphorylcholine bilayer saturated with cholesterol (POPC-Chol50) that models the bulk membrane; and (3) a Chol crystal. The computer model of the hydrated pure Chol bilayer is stable on the μs time scale. Some structural characteristics of Chol molecules in the Chol bilayer are similar to those in the POPC-Chol50 bilayer (e.g., tilt of Chol rings and chains), while others are similar to those in Chol crystals (e.g., surface area per Chol, bilayer thickness). The key result of this study is that the Chol bilayer has, unexpectedly, a dynamic structure, with Chol mobility similar to that in the POPC-Chol50 bilayer though slower. This is the major difference compared to Chol crystals, where Chol molecules are immobile. Also, water accessibility to Chol-OH groups in the Chol bilayer is not limited. On average, each Chol molecule makes 2.3 hydrogen bonds with water in the Chol bilayer, as compared with 1.7 hydrogen bonds in the POPC-Col50 bilayer.

### Keywords

cholesterol crystal; cholesterol bilayer domain; lipid mobility; eye lens

*Corresponding author: marta.pasenkiewicz-gierula@uj.edu.pl, Tel: (+48-12)-664-6518, Fax: (+48-12)-664-6902.

Supporting Information Available:

Time profiles showing the equilibration process of the Chol bilayer form the onset of MD simulation until 950 ns (Figure S1). The initial structure of the Chol bilayer was obtained based on the structure of a unit cell of the anhydrous cholesterol crystal[20]; time profiles showing the equilibration process of the Chol-2 bilayer for the time range of MD simulation between 0.5 and 200 ns (Figures S2). The initial structure of the Chol-2 bilayer was obtained by randomly rotating Chol molecules about their long axes and placing them in the *x,y*-plane in such a way that both bilayer surfaces were flat and the initial surface area of the simulation box was large, of 56.25 $nm^2$; time profiles of the bilayer potential energy and surface area, distributions of tilt angles of Chol rings and chains, $S_{mol}$ parameter profile for Chol chains, for the 4Chol and 4POPC-Chol50 bilayers; and water-Chol O-O RDF curves, for the Chol and POPC-Chol50 bilayers (Figures S3); snapshots of the initial and final lateral distributions (based on Voronoi tessellation) of lipid molecules in the POPC-Chol50 bilayers (Figure S4); collectivity of parallel rotation of neighboring Chol molecules in the Chol-2 and Chol bilayers (Figure S5); analysis of the wobble-in-cone type of motion of Chol C3-C17 vector in the Chol and POPC-Chol50 bilayers (Figure S6); simultaneous populations of angles by wobbling Chol molecules during 100 ns sampled with a 1 ps time step (Figure S7). This material is available free of charge via the Internet at http://pubs.acs.org.

## 1. Introduction

There is growing evidence that in model [1–6] and biological membranes [7–10] at high, oversaturating cholesterol (Chol) content, pure Chol domains are formed. These Chol domains have been illustrated as pure Chol bilayers surrounded by a bulk phospholipid bilayer containing Chol [6–7, 9–10], and in the literature, they have been called *cholesterol crystalline domains*, *cholesterol crystallites*, or, simply, *cholesterol crystals*. It is understood that these domains play a positive physiological role in the eye lens, helping to maintain lens transparency to visible light [7, 10–11], and, therefore, possibly preventing cataract formation [7, 9]. In other organs and tissues, appearance of these domains is usually a sign of pathology [9–10]. Better understanding of physiological functions of pure Chol domains requires increased understanding of Chol functions on a molecular level, including mechanisms of the formation of Chol-induced phases and domains in phospholipid membranes as well as characterization of these phases and domains. The latter has already achieved a good level of understanding (see recent review [12] and citations therein), however, significant discrepancy in interpretation of the results obtained by different experimental techniques regarding the structure and dynamics of the domains still exists.

Differential scanning calorimetry (DSC) [1–3] and X-ray diffraction [1, 13–14] measurements suggested that Chol domains formed in model and biological membranes possess the same properties as those found in one of three previously characterized triclinic Chol crystals (formed without phospholipids) [15]. These properties were periodic distance and phase transitions observed at 36 and 76°C. The controversial consequence of the crystal-like structure of the Chol domain was its rigidity and de- or low hydration. Recently, using electron paramagnetic resonance (EPR) spin-labeling methods we were able to show that in phospholipid bilayers oversaturated with Chol, Chol molecules form a bilayer-like domain with order and rotational motion of Chol molecules similar to those in the surrounding phospholipid bilayer saturated with Chol [16–18]. This bilayer-like structure differs from that of Chol crystals. Therefore, we have named the domain *cholesterol bilayer domain* (CBD) [16] to distinguish it from the *cholesterol crystalline domain*.

To further elucidate the nature of the cholesterol bilayer domain, we created computer models of the pure Chol fraction of a CBD using molecular dynamics (MD) simulations. This allowed for quantitative comparison of the organization and dynamics of Chol molecules in the pure Chol bilayer with those in the phospholipid bilayer saturated with Chol [19] and in Chol crystals [20–21]. Since our studies aim to shed some light on the role of Chol oversaturation in the eye lens membranes to build the computer bilayer models, we chose 2-palmitoyl-3-oleoyl-*D*-glycerol-1-phosphorylcholine (POPC) as the phospholipid and we did it for the following reasons: (1) the EPR experiments, which were the basis of this MD simulation study, were performed on bovine and porcine lens lipid membranes; (2) phosphatidylcholine (PC) is the most abundant phospholipid in bovine and porcine lenses, accounting for 31 to 46% of total lipids [22]; (3) palmitoyl and oleoyl are the major acyl chains of lens phospholipids of these animals, each representing ~34% of total chains [22–23]. Additionally, computer models of a POPC bilayer [24–25] as well as a POPC bilayer below saturation [26] and saturated with Chol [19] are well established and have been previously investigated in our lab.

In this study, we generated three computer models of the pure Chol fraction of a CBD, that is, a hydrated pure Chol bilayer. Two of them consisted of 200 Chol molecules and both were simulated for over 200 ns, but they differed in the initial configuration (Chol and Chol-2 bilayers) (*cf.* section 2.1). The third bilayer consisted of 800 Chol molecules; it was constructed by replicating the last frame of the Chol bilayer simulation over periodic boundaries (4Chol bilayer). This bilayer was simulated for over 75 ns. We also generated an

additional large computer model of a bulk membrane, that is, a POPC bilayer saturated with Chol from the POPC-Chol50 bilayer [19] (*cf.* section 2.1). The additional model consisted of 400 Chol and 400 POPC molecules; it was constructed by replicating the last frame of the POPC-Chol50 simulation over periodic boundaries (4POPC-Chol50 bilayer). This bilayer was simulated for over 75 ns.

The results of the comparison of all models used in this study unambiguously indicate that the pure Chol fraction of the CBD is a dynamic structure with Chol mobility similar to that in the phospholipid bilayer saturated with Chol and confirm experimental findings of the Subczynski's group [16–18].

## 2. Methods

### 2.1. System description

Initially, computer models of two lipid bilayers, each composed of 200 lipid molecules, were built. One bilayer comprised only Chol molecules (Chol bilayer), and the other, POPC and Chol molecules (Fig. 1) at a 1:1 molar ratio (POPC-Chol50 bilayer). The latter bilayer constituted a reference system. Each bilayer was hydrated with 6000 water molecules (30 $H_2O$/lipid). The construction and MD simulation of the POPC-Chol50 bilayer are described in Ref. [19].

The Chol bilayer was obtained based on the structure of a unit cell of the anhydrous Chol crystal as determined by Shieh *et al.* [20]. The unit cell consists of eight Chol molecules arranged in an "inverted" bilayer, in which the OH groups of four Chol molecules face the OH groups of the other four molecules related to them by pseudosymmetry. In the first step of building the bilayer, the unit cell was replicated in the *x,y*-plane in such a way as to construct an "inverted" bilayer of 10 × 10 × 2 Chol molecules. In the next step, the "inverted" bilayer was replicated along the *z*-axis, and the two outer leaflets were removed. After addition of hydrogen atoms to each Chol molecule, the constructed bilayer constituted the second reference system, the Chol crystal bilayer (shown in Figs 2a and c). After hydration, the bilayer was optimized and MD simulated using the GROMACSv4.0 software package [28]. A 560-ns MD simulation at standard conditions (see below) did not remove the initial ordered structure of the Chol crystal bilayer with the characteristic corrugated surface (Fig. 2a). To remove this regular crystal structure and surface roughness, the bilayer was simulated at an elevated temperature of 360 K for 146 ns. The temperature was then lowered back to 310 K (time profiles of the system temperature and potential energy are shown in Figs S1a and b, Supplementary Material). The simulation was continued until the bilayer surface area reached a stable value (Figs S1c, and d, Supplementary Material). Visual inspection indicated that the initial unevenness of the bilayer surface disappeared, and, thus, the configuration at 720 ns was considered to be the starting structure of the Chol bilayer.

To make sure that the properties of the Chol bilayer do not depend on its initial structure, a second Chol bilayer was built (Chol-2 bilayer; its initial structure is shown in Figs 2b and d). This bilayer also consisted of 10 × 10 × 2 Chol molecules that, in contrast to the Chol bilayer, were initially randomly rotated about their long axis (no crystal order in the initial structure) and were placed in the *x,y*-plane in such a way that both bilayer surfaces were flat (Fig. 2b), and the simulation box area was 56.25 $nm^2$, thus much larger than that of the Chol bilayer of 40 $nm^2$ (*cf.* Figs 2c and d).

### 2.2. Simulation parameters

Simulations of all bilayers were carried out in the *NPT* ensemble at a pressure of 1 atm and the physiological temperature of 310 K. The temperatures of the solute and solvent were controlled independently by the Nosé-Hoover method [29], with a relaxation time of 0.6 ps.

Pressure was controlled anisotropically by the Parrinello-Rahman method [30], with a relaxation time of 1.0 ps. The list of nonbonded pairs was updated every five time steps.

For POPC and Chol molecules, all-atom optimized potentials for liquid simulations (OPLS-AA) [31] with modifications of partial atomic charges on $CH_2$ and $CH_3$ groups of PC acyl chains described in Ref. [32] were used (unfortunately, these modifications were not acknowledged in Ref. [19], although they were implemented). For water, the transferable intermolecular potential three-point model (TIP3P) was used [33]. The linear constraint solver (LINCS) algorithm [34] was used to preserve the length of any covalent bond with a hydrogen atom, and the time step was set to 2 fs. The van der Waals interactions were cut off at 1.0 nm. Long-range electrostatic interactions were evaluated using the particle-mesh Ewald summation method [35] with a β-spline interpolation order of 5 and direct sum tolerance of $10^{-5}$. For the real space, a cutoff of 1.0 nm, three-dimensional periodic boundary conditions and the usual minimum image convention, were used [35]. The Chol, Chol-2, and POPC-Chol50 [19] bilayers were simulated for over 200 ns. Snapshots of the Chol, Chol-2, and POPC-Chol50 bilayers at the end of the respective 200-ns trajectories are shown in Figs 2e, f, g, and h.

After analyzing the results of the Chol and POPC-Chol50 simulations, we constructed and MD simulated two additional systems that were four times larger than the original Chol and POPC-Chol50 bilayers to rule out the possible effect of the system size on the obtained results. We created 4Chol and 4POPC-Chol50 bilayers by replicating the last frame of the respective MD simulations over periodic boundaries, thus, each bilayer comprised 800 lipids. All simulation parameters and conditions were the same as for the original bilayers, except for simulation times, which were 75 ns.

## 3. Results and Discussion

### 3.1. Characterization of the membranes

**3.1.1. Equilibration—**The first indicator of thermal equilibration of the lipid bilayer is the convergence of the bilayer's potential energy and surface area. Time profiles of the Chol bilayer's potential energy and surface area, together with those for the POPC-Chol50 bilayer, from the onset of simulation until 200 ns are shown in Figs 3a and b, respectively. The figures do not include data from the process of breaking the initial regular structure of the Chol bilayer. Time profiles for this process are shown in Fig. S1 (Supplementary Material). Figs 3a and b indicate that the Chol bilayer is practically well-equilibrated from the onset (which corresponds to the 720$^{th}$ ns of the total simulation process) of MD simulation. Also, time profiles of the potential energy and surface area of the Chol-2 bilayer shown in Fig. S2 (Supplementary Material) illustrate that this bilayer reaches thermal equilibrium in ~50 ns of MD simulation. Because the POPC-Chol50 bilayer stabilized only within 80 ns [19] for further analyses, the last 100-ns fragment of the trajectory generated in the 200 ns MD simulation of each bilayer was used.

Stability of the system's potential energy and the surface area of the simulation box are not totally convincing indicators of thermal equilibration of the Chol bilayers. However, further argument for the thermal equilibration provides the comparison of top views of the Chol and Chol-2 bilayers (Figs 2c, d, e, and f), and side views of the Chol bilayer (Figs 2a and h) at the beginning and the end of their MD simulations. This comparison indicates that in the course of MD simulations, the bilayers lost their initial positional order and individual Chol molecules changed their orientations. Moreover, as it will be shown in Results and Discussion below, even though the translational motion of Chol molecules in the bilayers is slow, on the 100 ns time scale, the molecules undergo free rotation about their long molecular axes, and their long molecular axes wobble about their preferred orientation;

additionally, rotation about long molecular axes of neighboring Chol molecules in the Chol-2 and Chol bilayers is only modestly correlated. This indicates that most of Chol molecules practically "forget" their initial orientation in the bilayer within ~100 ns, *i.e.*, in a time comparable to the equilibration simulation time of 100 ns. One might thus expect that neither the POPC-Chol50 nor the Chol bilayers are stuck in some metastable configurations.

4Chol and 4POPC-Chol50 bilayers were built from bilayers generated in 200-ns MD simulations, thus thermally equilibrated; nevertheless, the first 25 ns fragments of the respective MD trajectories were excluded from the analyses below. Time profiles of their potential energy and surface area from the onset of simulation until 75 ns are shown in Figs S3a and b (Supplementary Material).

Snapshots of the initial and final lateral distributions of lipid molecules in the POPC-Chol50 bilayers (Fig. S4, Supplementary Material) indicate that the Chol and POPC molecules are homogeneously distributed in the bilayers also at the end of MD simulations (their initial distributions were homogeneous, Fig. S4a). This is consistent with the phase diagram for a PC-Chol bilayer where between ~30 and 50 mol% Chol, a single liquid ordered phase is present[36] and indicates that the models correctly reproduce experimental systems.

The values reported below for Chol, Chol-2, and POPC-Chol50 bilayers are time averages over the last 100-ns fragment of the respective trajectory and for 4Chol and 4POPC-Chol50 bilayers, over the last 50-ns fragment of the respective trajectory, and the ensemble of molecules or their fragments. Errors in the derived average values are standard deviation estimates, and in the case of $S_{mol}$, standard error estimates.

**3.1.2. Membrane thickness and cross-sectional area per lipid—**Thickness of the phospholipid bilayer is generally evaluated as the distance between the average positions of phosphorus (P) atoms in the two leaflets of a bilayer (P-P distance). P-P distances for the POPC-Chol50 [19] and 4POPC-Chol50 bilayers are given in Table 1. Thickness of the Chol bilayer was evaluated as the distance between the average positions of Chol C3 atoms (see Fig. 1b) in the two leaflets of the bilayer (C-C distance); C-C distances for the Chol, Chol-2, and 4Chol bilayers are given in Table 1 together with those for the POPC-Chol50 and 4POPC-Chol50 bilayers and for the Chol crystal bilayer (Table 1). The P-P distances in both POPC-Chol50 and 4POPC-Chol50 bilayers, of ~45.7 Å are practically the same, also the C-C distances in the Chol, Chol-2, and 4Chol bilayers, of ~32 Å are practically the same. An average cross-sectional area per Chol ($A_{Chol}$) in the Chol bilayer, was obtained by dividing the area of the simulation box by the number of Chol molecules present in one bilayer leaflet (geometric area); $A_{Chol}$ values for the Chol, Chol-2, and 4Chol bilayers are given in Table 1. The values of $A_{Chol}$ in the three bilayers are practically the same, of ~38 $Å^2$ and are very close to $A_{Chol}$ values in the Chol crystal of ~37 $Å^2$ [20], and in a Chol monolayer of ~39 $Å^2$ [37]. The average surface area per POPC ($A_{PC}$) in the POPC-Chol50 and 4POPC-Chol50 bilayers was obtained by subtracting the mean cross-sectional area of, respectively, 50 or 200 Chol molecules (50(200) × 38.0 $Å^2$) from the total surface area of the simulation box and then dividing it by the number of POPC molecules present in one bilayer leaflet [38–39]. $A_{PC}$ values for the POPC-Chol50 and 4POPC-Chol50 bilayers, of ~48$Å^2$, are the same (Table 1). The concept of geometric area basically differs from that of partial-specific-area introduced by Edholm and Nagle[40] that additionally requires simulations of PC-Chol bilayers at several cholesterol concentrations. Thus, $A_{Chol}$ calculated in this paper should not be confused with $A_{Chol}$ calculated in Edholm and Nagle[40]. Nevertheless, the values of $A_{PC}$ obtained by both approaches for PC-Chol bilayers containing 50 mol% Chol simulated in this study and that of Edholm and Nagle[40], are very similar.

**3.1.3. Tilt of Chol ring and chain—**The POPC-Chol50 bilayer containing 50 mol% Chol is in the liquid-ordered phase. As the Chol molecules in the Chol bilayer possess rotational and translational freedom (see below), we can by analogy assume that the Chol bilayer is in the phase similar to the liquid-ordered. In this phase, there is no collective tilt of either the acyl chains or steroid rings. Indeed, due to rotational freedom of Chol molecules in an axially symmetric system, distribution of azimuthal angles $\varphi$ (see below) of the Chol long axis is uniform in the full range of angles (Fig. 3e), thus the average (over the whole range) angle of Chol rings (and chains) with respect to the bilayer normal ($\theta$ angle) is zero. However, due to the rotation about axes perpendicular to the bilayer normal, the rings as well as the chains, are generally tilted relative to the normal within a limited range of angles. In this study, because of its comparative character (no direct comparison with experimental values of tilt), the tilt angle $\theta$ is simply the absolute value of the polar angle $\theta$. The tilt angle $\theta$ of the Chol ring and chain was calculated from the scalar product of the vector linking the C3 and C17 atoms (see Fig. 1b) in the case of rings, and the C17 and C25 atoms in the case of chains, and the bilayer normal ($arccos\theta$). The azimuthal angle $\varphi$ was calculated from the scalar product of the projection of the C3-C17 vector on the *x,y*-plane and the *x*-axis. Distributions of the tilt angles of the Chol rings and chains in the Chol, Chol-2, and POPC-Chol50 bilayers are shown in Figs 3c and d, respectively, and for the 4Chol and 4 POPC-Chol50 bilayers in Figs S3c and d (Supplementary Material), respectively. The distributions in Figs 3c and S3c are very similar to that obtained in Ref. [41] for a PC-Chol bilayer at1:1 molar ratio where both PC acyl chains were saturated. Distributions of the $\varphi$ angles of the Chol rings in the Chol and POPC-Chol50 bilayers are shown in Fig. 3e. The most probable, the average (calculated from the distribution), and the standard deviation values of the tilts are given in Table 1. The vertical lines in Figs 3c, d, S3c, and d represent respective tilts for the eight Chol molecules in the unit cell of the anhydrous Chol crystal [20]; the tilts are 9.2°, 16.3°, 17.9°, 18.2°, 20.4°, 21.2°, 34.8°, 35.0° for the rings, and 9.0°, 12.6°, 13.0°, 17.1°, 19.8°, 22.2°, 22.6°, 27.1° for the chains. The most probable tilts of the Chol rings and chains are similar in all simulated systems, irrespectively of their initial structures and sizes (Table 1, Figs 3c, d, S3c, and d); the distribution of ring tilts is slightly broader in the POPC-Chol50 bilayers (Figs 3c and S3c), whereas the distribution of chain tilts is narrower (Figs 3d and S3d) than in all Chol bilayers. The most probable values of tilts in all bilayers (~8–9° for rings and ~13° for chains) are much lower than most of the tilt values in the Chol crystal. The broad range of Chol tilts in the unit cell of the anhydrous Chol crystal[20] allows formation of infinite chains of intermolecular hydrogen bonds[20–21] and induces a similar density of packing of the Chol molecules as in the hydrated Chol bilayer, where the molecules are much less tilted.

**3.1.4. Chain order—**The measure of a hydrocarbon chain order in a lipid bilayer—both experimentally (*e.g.*, see Ref. [42]) and computationally (*e.g.*, see Ref. [43])—is the order parameter. The molecular order parameter for the $n$th segment of an acyl chain, $S_{mol}$, is defined by [44]

$$S_{mol}=\frac{1}{2}\left\langle 3\cos^2\theta_n-1\right\rangle, \quad (1)$$

where $\theta_n$ is the instantaneous angle between the $n$th segmental vector (*i.e.*, the ($C_{n-1}$, $C_{n+1}$) vector linking $n-1$ and $n+1$ C atoms in the acyl chain) and the bilayer normal, and $\langle\cdots\rangle$ denotes both the ensemble and the time average. There are five consecutive segmental vectors in the Chol chain, the first is between C17 and C22, and the fifth is between C24 and C26 (*cf.* Fig. 1b). $S_{mol}$ profiles along this chain in the Chol, Chol-2, and POPC-Chol50 bilayers are shown in Fig. 3f, and in the 4Chol and 4POPC-Chol50 bilayers in Fig. S3e (Supplementary Material). Mean values of $S_{mol}$ obtained by averaging over all segmental

$S_{mol}$ values are given in Table 1. It can be seen from the figures and the table that both the profiles and mean values of $S_{mol}$ are practically the same for all Chol (POPC-Chol50) bilayers, irrespectively of their initial structure and sizes; also that order of Chol chains in the Chol bilayers is visibly lower than in the POPC-Chol50 bilayer. The latter is in line with the result of the tilt angle analysis of Chol chains. Higher order and narrower distribution of tilt angles (see above) of Chol chains in the POPC-Chol50 bilayers imply that Chol chains have less motional freedom in the POPC-Chol50 than the pure Chol bilayers because of smaller available space. The bulky and rigid steroid Chol rings create "free volume" in the central part of the bilayer. In the Chol bilayer, this volume is occupied only by the Chol chains, whereas, in the POPC-Chol 50 bilayer, it is also occupied by the fragments of PC acyl chains that extend further into the bilayer than the Chol rings, *i.e.*, by the fragments below the 10th carbon atom. Thus, one can say that in the POPC-Chol50 bilayer, PC acyl chains have an ordering effect on Chol chains.

The C-C distance, $A_{Chol}$, most probable tilt, and average $S_{mol}$ values for the 4Chol and 4POPC-Chol50 bilayers are practically the same as the respective values obtained for the initial smaller systems (Table 1). Thus, most analyses of Chol dynamics in the Chol and POPC-Chol50 bilayers were carried out only for the smaller systems. Moreover, the analyses of Chol dynamics were carried out mainly on the Chol-2 rather than Chol bilayer even though the "static" properties of both bilayers were practically the same. Such a choice was motivated by apparently less ordered structure of the Chol-2 bilayer (*cf.* Figs 2e and f) that resulted from the way of its construction (large surface area of its initial configuration, the lack of the initial positional order, *cf.* Figs 2b and d). More random orientations of Chol molecules in the bilayer should yield more statistically significant results of analyses of rotational dynamics due to a broader variety of initial orientations of rotating molecules over which averaging takes place.

### 3.2. Translational mobility of Chol molecules in the bilayer

**3.2.1. Lateral diffusion—**Lateral mobility of lipid molecules in the bilayer was estimated by calculating the two-dimensional mean square displacement (MSD) as a function of time, defined by

$$MSD(t)=\langle|r(t_0)-r(t_0+t)|^2\rangle \quad (2)$$

where $r(t_0)$ is the position of the center of mass (CM) of a lipid molecule in the $x,y$-plane at the initial time, $t_0$; $t$ is sampled with 10 ps time steps, and $<\cdots>$ denotes the ensemble average. $MSD(t)$ was averaged over 100 lipid molecules in the Chol, Chol-2 and POPC-Chol50 bilayers and 400 lipid molecules in the 4Chol and 4POPC-Chol50 bilayers, and additionally over 250 initial times (running average). MSDs were calculated for a lag time $\tau$ = 10 ns, *i.e.*, $t$ in eq. 2 changed from 0 to $\tau$, and MSD curves for the Chol-2 and POPC-Chol50 bilayers are shown in Fig. 4a. The values of MSD for $t = \tau$ = 10 ns for Chol and POPC molecules in respective bilayers are given in Table 1. An error of each MSD for $t$ = 10 ns was calculated from the distribution of MSDs of individual lipid molecules (molecular MSDs). As the lipids in the bilayer undergo an anomalous diffusion [45], the diffusion coefficient for the lateral self-diffusion, $D$, cannot be obtained from the linear part of the MSD curve, as is the case for a simple Brownian diffusion. Instead, the fractional diffusion coefficient may be obtained, but only by curve fitting [45]. However, in this study, we are only interested in qualitative comparison of Chol mobility in two environments, and not in numerical values of fractional diffusion coefficients. Therefore they were not calculated. The mean distance that the lipid molecules, on average, covered during the lag time was calculated as the square root of the MSD for $t = \tau$. The mean distances covered during 10 ns by the Chol molecules were 2.4 ± 1.1, 2.4 ± 1.6, and 2.7 ± 1.8 Å in the Chol, 4Chol, and

Chol-2 bilayers, respectively, and 3.6 ± 2.2, and 3.7 ± 2.1 Å in the POPC-Chol50 and 4POPC-Chol50 bilayers, respectively. For comparison, the mean distances covered during 10 ns by the POPC molecules were 4.3 ± 2.2 and 4.5 ± 2.2 Å in the POPC-Chol50 and 4POPC-Chol50 bilayers, respectively. These numbers, together with the curves in Fig. 4a, as well as relevant entries in Table 1, indicate that Chol molecules are laterally mobile both in POPC bilayers containing saturating amount of Chol and in pure Chol bilayers, though, due to the dense packing of molecules in the bilayers, their motion is slow and in the pure Chol bilayers it is slower than in the POPC-Chol50 bilayers. If the further lateral diffusion of Chol molecules were simple Brownian, then during 200 ns, Chol molecules would, on average, translocate a distance of ~11 Å in the Chol bilayer, and ~16 Å in the POPC-Chol50 bilayer, however, in the case of anomalous diffusion, the distances are considerably less. It is interesting to note that POPC molecules in the POPC-Chol50 bilayer seem to translocate faster than Chol molecules. However, this may be a result of their much higher intramolecular conformational mobility.

**3.2.2. Vertical diffusion—**Vertical mobility of Chol molecules in the Chol-2 and POPC-Chol50 bilayers was estimated in an analogous way, as was lateral mobility (*i.e.*, using eq. 2 in one dimension, *i.e.* along the *z*-axis). This vertical motion is spatially restricted—on the upper side by the water phase, which is an unfavorable environment for the nonpolar core of the Chol molecule, and on the lower side by the hydrophobic core of the bilayer, which is an unfavorable environment for the polar Chol OH group. MSDs for the vertical self-diffusion of CMs of 100 Chol molecules in the Chol-2 and POPC-Chol50 bilayers were calculated for the lag time $\tau = 30$ ns ($t$ changes from 0 to $\tau$) and are shown in Fig. 4b. MSD curves for both bilayers reached almost the same plateau value of ~0.06 $nm^2$, however, at different times, ~15 ns for the POPC-Chol50 bilayer and ~23 ns for the Chol-2 bilayer. This means that Chol molecules in both bilayers cover an average vertical distance limited to ~2.5 Å, which can be considered an allowed “average spatial zone” of vertical fluctuations.

## 3.3. Rotational mobility of Chol molecules in the bilayer

### 3.3.1. Parallel rotation

Rotation of a lipid molecule about the long molecular axis is called the *parallel rotation*. The long molecular Chol axis is defined by the C3-C17 vector (see Fig. 1b). The parallel rotational diffusion was estimated by calculating the normalized time rotational autocorrelation function (RAF) of the projection of the Chol C13-C18 bond (see Fig. 1b); this bond is perpendicular to the steroid ring and thus to the C3-C17 vector. RAF is defined by

$$RAF(t)=\frac{\langle v(t_0)\cdot v(t_0+t)\rangle}{|v(t_0)||v(t_0+t)|}, \quad (3)$$

where $v(t_0)$ is the projection of the C13-C18 vector on the *x,y*-plane at the initial time, $t_0$; $t$ is sampled with 1 ps time steps, and $\langle\cdots\rangle$ denotes the ensemble average. Thus, the function is the ensemble averaged scalar product of the vector at time $t$ with itself at time $t_0$. Normalization in eq. 3 accounts for changes of the magnitude of the projection of the C13-C18 vector on the *x,y*-plane with time. RAFs were calculated for 100 Chol molecules in the Chol-2 and POPC-Chol50 bilayers for the lag time $\tau = 100$ ns ($t$ changes from 0 to $\tau$). Additionally, they were averaged over 1000 initial times and are shown in Fig. 4c. Errors in RAFs were calculated in a similar way as those in MSDs. For random processes, RAF most often decays exponentially. For the POPC-Chol50 bilayer, the RAF decays from 1.0 to 0.02 ± 0.22 within ~50 ns, and then retains the average value of 0.01 ± 0.25 for the next 50 ns of the analysis time, whereas for the Chol bilayer, it decays to 0.09 ± 0.43 within ~100 ns (it

reached zero after next 50 ns, results not shown). These numbers indicate that both in the Chol-2 and POPC-Chol50 bilayers, the parallel rotation of Chol molecules about their molecular axes is an unrestricted angular diffusion.

Collectivity of parallel rotation of neighboring Chol molecules in the Chol-2 bilayer was evaluated by calculating a simple correlation function. In the first step, three Chol molecules located in different parts of the Chol-2 bilayer were chosen (Fig. S5a, Supplementary Material). Next, for each of the three Chol molecules, a 70-ns time profile (sampled with 70 ps time steps) of the cosine of the change ($\Delta\beta$) in the angle ($\beta$) between the projection of the C13-C18 bond on the *x,y*-plane and that of each of its six nearest neighbors, relative to the initial $\beta_0$, was calculated. Each profile was averaged over 1000 initial times and then over six pairs. The average of the three profiles is shown in Fig. S5c (Supplementary Material). The profile in Fig. S5c indicates that the parallel rotation of a Chol molecule in the Chol-2 bilayer is not strongly correlated with that of its near-neighbors and also that the initial decay of the correlation is rapid. A similar result was obtained for the Chol bilayer (Fig. S5d, Supplementary Material).

Fig. 5 shows simultaneous populations of $\alpha$ and $\theta$ angles (defined below) by rotating Chol molecules during 100 ns sampled with a 1 ps time step for two Chol molecules in the POPC-Chol50 and Chol-2 bilayers. In each bilayer, one of the molecules belongs to the ones most mobile about the long axis, and the other to the ones least mobile about the long axis. The angle $\alpha$ is between the projection of the C13-C18 vector on the *x,y*-plane and the *x*-axis; the angle $\theta$ is between the C13-C18 vector and the *x,y*-plane (that is, between the C3-C17 vector and the bilayer normal = tilt angle). The populations of $\alpha$ angles in Fig. 5 indicate that both in the Chol-2 and in POPC-Chol50 bilayers parallel rotational mobility of the Chol molecules is large. It is interesting to note (Fig. 5) that the rotation of Chol molecules about their long axes is rather a series of jumps between confined ranges of $\alpha$ than continuous diffusion, particularly in the Chol-2 bilayer, and also that in both Chol-2 and POPC-Chol50 bilayers, the rotation of some Chol molecules about the long axis is confined to a range of $\alpha$ of ~120° for at least 100 ns.

**3.3.2. Perpendicular rotation—**Rotation of a lipid molecule about the axis perpendicular to the long molecular axis is called the *perpendicular rotation*. In principle, there is an infinite number of perpendicular axes about which a Chol molecule can rotate in the bilayer ($\varphi$ angle is not restricted; *cf.* section 3.1.3, Figs 3e, and S7, Supplementary Material). Such a rotation is named wobbling-in-cone and is described in detail by Kinosita *et al.* [46–47]. In this type of motion, perpendicular rotation relative to the cone axis (an initial tilt of the long axis) cannot be separated from the transient precession of the long axis itself —both motions are coupled and interdependent. In this analysis, the perpendicular rotational diffusion is estimated by calculating RAF of the projection of the Chol C3-C17 vector (see Fig. 1b) on the bilayer normal using eq. 3 in a way analogous to that for the parallel rotation, where $v(t_0)$ is now the projection of the C3-C17 vector at the initial time, $t_0$. Such geometry implies that perpendicular rotation is actually calculated relative to the initial tilt of the Chol long axis (Chol ring). RAFs for the Chol-2 and POPC-Chol50 bilayers are shown in Fig. 4d (and also in Fig. S6b, Supplementary Material). It is apparent from the decay curves in Fig. 4d that the perpendicular rotation of Chol is really restricted in both bilayers—RAF decays from 1.0 to 0.989 ± 0.003 in the Chol-2 bilayer and to 0.990 ± 0.004 in the POPC-Chol50 bilayer. Decay of the RAFs from 1 to 0.99 means that the angular amplitude of wobbling of the C3-C17 vector about its initial tilt, both in the Chol-2 and POPC-Chol50 bilayers, is 8.1° [arcos(0.99)]. Moreover, the inset of Fig. 4d shows that RAF for the POPC-Chol50 bilayer decays to a constant (0.99 ± 0.004) within ~2 ns; this in turn indicates that the perpendicular rotation is fast.

As has been already mentioned above, this perpendicular rotation relative to the cone axis cannot be separated from the transient precession of the long axis itself. The latter rotation was estimated by calculating RAF of the projection of the Chol long molecular axis (C3-C17 vector) on the *x,y*-plane. The RAFs for the POPC-Chol50 and Chol-2 bilayers are shown in Fig. S6a (Supplementary Material). From the decay pattern of the RAFs both in Fig. S6a and b (Supplementary Material) one can conclude the wobbling is significantly faster in the POPC-Chol50 than in the Chol-2 bilayer.

The curves in Fig. S6a (Supplementary Material) prove that motion of the C3-C17 vector is free wobbling—both curves decay to zero (though at different times), which implies that the majority of angles within the cone are populated by the C3-C17 vector. Additional support for the free wobbling provides analysis of simultaneous populations of $\varphi$ and $\theta$ angles by the rotating C3-C17 vector (the $\theta$ angle is between the projection of the C3-C17 vector on the *x,y*-plane and the *x*-axis, and $\theta$ is the tilt angle) in Fig. S7 (Supplementary Material)—within 100 ns, $\varphi$ populated the whole range of angles, while $\theta$ populated a confined range of angles. Moreover, the initial rapid decay of RAFs in Figs S6a and b illustrate the fact that for wobbling, changes in $\theta$ cannot be separated from changes in $\varphi$—rapid changes in $\theta$ (inset of Fig. S6b) trigger rapid changes in $\varphi$ (inset of Fig. S6a); for more details, see legend to Fig. S6 (Supplementary Material).

The value of the angular amplitude of wobbling of 8.1° obtained in the RAF analysis is consistent with the spread of the populations of $\theta$ angles in Figs 5 and S7 (Supplementary Material) of ~15°. On the other hand, the populations of $\theta$ angles and the angular amplitude of wobbling of 8.1° are in overall agreement with the result of the tilt angle analysis of Chol rings—in both bilayers the most probable tilts are similar and small and their distributions are relatively narrow (Fig. 3c, Table 1).

Motional behavior of Chol molecules in the pure Chol bilayer and in the POPC bilayer saturated with Chol can be summarized as follows. The lateral and vertical diffusion of Chol molecules take place in both bilayers (Figs 4a and b). Diffusion is slow in both bilayers but slower in the Chol than the POPC-Chol50 bilayers, whereas the spatial range in which the vertical diffusion takes place is the same. In contrast to translational diffusion, rotational motion of Chol molecules is substantial. They fully rotate about their long molecular axes (parallel rotation, $\alpha$ angle, Fig. 4). In agreement with previous experimental studies[48], their perpendicular rotation is free wobbling-in-cone [46–47] ($\varphi$ and $\theta$ angles, Fig. S6, Supplementary Material) with the initial tilt as the cone axis and the semi cone angle of 8.1°; this motion is relatively fast. To better illustrate rotational motions, populations of angles for selected Chol molecules are shown in Fig. 5 and Fig. S7 (Supplementary Material). As in the case of the translational diffusion, rotational diffusion of the Chol molecules in the pure Chol bilayer is slower than in the POPC-Chol50 bilayer.

### 3.4. Cholesterol-water hydrogen bonds

To determine whether Chol in the bilayer interacts with water, a radial distribution function (RDF) of the oxygen atoms of water and Chol (O-O RDF) was calculated for the Chol and POPC-Chol50 bilayers (Fig. S3f, Supplementary Material). The position of the first peak in RDF of ~0.27 nm (Fig. S3f) indicates formation of hydrogen (H-) bonds between the Chol OH group and water in both bilayers. To compare the extent of H-bonding in each bilayer, the number of H-bonds was calculated using the following geometric criteria: the distance between the water oxygen atom (Ow) and the Chol oxygen atom (Och) is ≤ 0.35 nm, and the angle between the Ow-Och vector and the O-H bond is ≤ 30°. [49] The numbers of Chol· · ·water H-bonds per Chol are ~2.3 in the Chol, Chol-2, and 4Chol bilayers (Table 1), and ~1.7 in the POPC-Chol50 and 4 POPC-Chol50 bilayers (Table 1). The latter number is higher than the number of Chol· · ·water H-bonds per Chol in a bilayer containing PCs with

saturated acyl chains and ~22 mol % of Chol (or an epimeric form of Chol, epicholesterol) of ~0.8 ± 0.1. [50] The maximum expected average number of H-bonds/Chol is three (two with Och and one with Hch), so Chol molecules in the pure Chol bilayer make close to the maximal number of H-bonds with water.

The presence of pure Chol domains in bilayers oversaturated with Chol and an extensive H-bonding between Chol OH group and water molecules in the domains might seem at variance with the "umbrella model" [51–52]. The model states that in a PC-Chol bilayer, PC headgroups neighboring Chol molecules are expected to cover the hydrophobic body of cholesterol molecules to reduce their exposure to water. In our previous studies [38, 53] as well as in that of Pandit *et al.* [54], it was shown that indeed, in the interfacial bilayer region, there is a short-range interaction between a (positively charged) choline group of PC and an (negatively charged) oxygen atom of the Chol OH group. This interaction probably causes the inward orientation (toward the bilayer center) of the PC choline group and a more horizontal orientation of the PC α-chain in a PC bilayer containing Chol, observed by Tu et al. [55] and Seelig and Seelig [42]. But such an orientation of the PC α-chain does not prevent Chol molecules from making H-bonds with water in a PC-Chol bilayer [38, 54, 56]. The "umbrella model" does not allow for the formation of pure Chol domains in a PC-Chol bilayer. However, the present study demonstrates that a computer model of the hydrated (30 water molecules per Chol) pure Chol bilayer parameterized by OPLS-AA and TIP3P force fields (*cf.* Methods section) is stable on the μs time scale (Figs S1 and S3a and b, Supplementary Material). We certainly cannot say how much longer this bilayer is stable. Neither can we say what might be the size and shape of a pure Chol domain in the bilayer oversaturated with Chol in the case when such a domain really forms, nor what is its lifetime. Nevertheless, this simulation does not exclude the possibility that once a cholesterol bilayer domain is formed, it can exist on the μs time scale and possibly longer.

## 4. Conclusions

In this computer simulation study, stable computer models of a hydrated pure Chol bilayer ($30H_2O$/Chol) were generated. The behavior of Chol molecules in the pure Chol bilayers was compared with that in the POPC-Chol50 bilayers containing 50 mol% Chol and in the Chol crystal. The key finding of this study is the demonstration that Chol molecules in the Chol bilayers are mobile and they undergo both translational and rotational motion.

Motion of Chol molecules in the Chol bilayers is slower than in the POPC-Chol50 bilayers, but in the crystal, Chol molecules are fixed in their positions and, thus, totally immobile. Altogether, Chol molecules in the Chol bilayers behave similarly to those in the POPC bilayers saturated with Chol. The second key result of this study is the estimation of the number of Chol· · ·water H-bonds in the Chol bilayers as 2.3. This number is close to 3, the expected maximal number of such H-bonds, but significantly greater than 1.7, the number of H-bonds between Chol and water in POPC-Chol50 bilayers.

The results of this study strongly support the conclusions of experimental EPR spin-labeling studies [16–17] which suggest that pure Chol domains that form in PC bilayers oversaturated with Chol are hydrated bilayers (CBDs) where Chol molecules possess motional freedom—both translational and rotational—and are exposed to excess water. Anhydrous and monohydrated organized structures of Chol detected by other experimental techniques [1–3, 6], most likely form outside the lipid bilayer and cannot be identified with pure Chol bilayer domains within the lipid bilayer.

## Supplementary Material

Refer to Web version on PubMed Central for supplementary material.

## Acknowledgments

This work was supported by grants TW008052 and EY015526 of the National Institutes of Health. Some calculations were performed on the cluster purchased under contract No. POIG.02.01.00-12-167/08, project MCB.

## References

1. Wachtel EJ, Borochov N, Bach D. The Effect of Protons or Calcium Ions on the Phase Behavior of Phosphatidylserine-Cholesterol Mixtures. Biochim Biophys Acta. 1991; 1066:63–9. [PubMed: 1648395]
2. Borochov N, Wachtel EJ, Bach D. Phase Behavior of Mixtures of Cholesterol and Saturated Phosphatidylglycerols. Chem Phys Lipids. 1995; 76:85–92. [PubMed: 7788803]
3. Epand RM. Cholesterol in Bilayers of Sphingomyelin or Dihydrosphingomyelin at Concentrations Found in Ocular Lens Membranes. Biophys J. 2003; 84:3102–3110. [PubMed: 12719240]
4. Knoll W, Schmidt G, Ibel K, Sackmann E. Small-Angle Neutron-Scattering Study of Lateral Phase-Separation in Dimyristoylphosphatidylcholine Cholesterol Mixed Membranes. Biochemistry. 1985; 24:5240–5246. [PubMed: 4074692]
5. Guo W, Hamilton JA. C-13 Mas Nmr Studies of Crystalline Cholesterol and Lipid Mixtures Modeling Atherosclerotic Plaques. Biophys J. 1996; 71:2857–2868. [PubMed: 8913623]
6. Ziblat R, Leiserowitz L, Addadi L. Crystalline Domain Structure and Cholesterol Crystal Nucleation in Single Hydrated Dppc:Cholesterol:Popc Bilayers. J Am Chem Soc. 2010; 132:9920–7. [PubMed: 20586463]
7. Jacob RF, Cenedella RJ, Mason RP. Direct Evidence for Immiscible Cholesterol Domains in Human Ocular Lens Fiber Cell Plasma Membranes. J Biol Chem. 1999; 274:31613–31618. [PubMed: 10531368]
8. Jacob RF, Cenedella RJ, Mason RP. Evidence for Distinct Cholesterol Domains in Fiber Cell Membranes from Cataractous Human Lenses. J Biol Chem. 2001; 276:13573–13578. [PubMed: 11278611]
9. Tulenko TN, Chen M, Mason PE, Mason RP. Physical Effects of Cholesterol on Arterial Smooth Muscle Membranes: Evidence of Immiscible Cholesterol Domains and Alterations in Bilayer Width During Atherogenesis. J Lipid Res. 1998; 39:947–56. [PubMed: 9610760]
10. Mason RP, Jacob RF. Membrane Microdomains and Vascular Biology - Emerging Role in Atherogenesis. Circulation. 2003; 107:2270–2273. [PubMed: 12732593]
11. Borchman D, Cenedella RJ, Lamba OP. Role of Cholesterol in the Structural Order of Lens Membrane Lipids. Exp Eye Res. 1996; 62:191–197. [PubMed: 8698079]
12. Subczynski WK, Raguz M, Widomska J, Mainali L, Konovalov A. Functions of Cholesterol and the Cholesterol Bilayer Domain Specific to the Fiber-Cell Plasma Membrane of the Eye Lens. J Membr Biol. 2012; 245:51–68. [PubMed: 22207480]
13. Cheetham JJ, Wachtel E, Bach D, Epand RM. Role of the Stereochemistry of the Hydroxyl Group of Cholesterol and the Formation of Nonbilayer Structures in Phosphatidylethanolamines. Biochemistry. 1989; 28:8928–8934. [PubMed: 2557911]
14. Mason RP, Tulenko TN, Jacob RF. Direct Evidence for Cholesterol Crystalline Domains in Biological Membranes: Role in Human Pathobiology. Biochim Biophys Acta-Biomem. 2003; 1610:198–207.
15. Loomis CR, Shipley GG, Small DM. The Phase Behavior of Hydrated Cholesterol. J Lipid Res. 1979; 20:525–35. [PubMed: 458269]
16. Raguz M, Mainali L, Widomska J, Subczynski WK. The Immiscible Cholesterol Bilayer Domain Exists as an Integral Part of Phospholipid Bilayer Membranes. Biochim Biophys Acta. 2011; 1808:1072–80. [PubMed: 21192917]
17. Raguz M, Mainali L, Widomska J, Subczynski WK. Using Spin-Label Electron Paramagnetic Resonance (Epr) to Discriminate and Characterize the Cholesterol Bilayer Domain. Chem Phys Lipids. 2011; 164:819–829. [PubMed: 21855534]

18. Mainali L, Raguz M, Subczynski WK. Phases and Domains in Sphingomyelin-Cholesterol Membranes: Structure and Properties Using Epr Spin-Labeling Methods. Eur Biophys J. 2012; 41:147–59. [PubMed: 22033879]
19. Plesnar E, Subczynski WK, Pasenkiewicz-Gierula M. Saturation with Cholesterol Increases Vertical Order and Smoothes the Surface of the Phosphatidylcholine Bilayer: A Molecular Simulation Study. Biochim Biophys Acta Biomem. 2012; 1818:520–529.
20. Shieh HS, Hoard LG, Nordman CE. The Structure of Cholesterol. Acta Crystallogr B. 1981; 37:1538–1543.
21. Craven BM. Pseudosymmetry in Cholesterol Monohydrate. Acta Crystallogr B. 1979; 35:1123–1128.
22. Deeley JM, Mitchell TW, Wei X, Korth J, Nealon JR, Blanksby SJ, Truscott RJ. Human Lens Lipids Differ Markedly from Those of Commonly Used Experimental Animals. Biochim Biophys Acta. 2008; 1781:288–298. [PubMed: 18474264]
23. Li LK, So L, Spector A. Membrane Cholesterol and Phospholipids in Consecutive Concentric Sections of Human Lenses. J Lipid Res. 1985; 26:600–609. [PubMed: 4020298]
24. Murzyn K, Rog T, Jezierski G, Takaoka Y, Pasenkiewicz-Gierula M. Effects of Phospholipid Unsaturation on the Membrane/Water Interface: A Molecular Simulation Study. Biophys J. 2001; 81:170–83. [PubMed: 11423404]
25. Rog T, Murzyn K, Gurbiel R, Takaoka Y, Kusumi A, Pasenkiewicz-Gierula M. Effects of Phospholipid Unsaturation on the Bilayer Nonpolar Region: A Molecular Simulation Study. J Lipid Res. 2004; 45:326–336. [PubMed: 14594994]
26. Rog T, Pasenkiewicz-Gierula M. Cholesterol Effects on a Mixed-Chain Phosphatidylcholine Bilayer: A Molecular Dynamics Simulation Study. Biochimie. 2006; 88:449–460. [PubMed: 16356621]
27. Sundaralingam M. Molecular Structures and Conformations of the Phospholipids and Sphingomyelins. Ann NY Acad Sci. 1972; 195:324–355. [PubMed: 4504096]
28. Hess B, Kutzner C, van der Spoel D, Lindahl E. Gromacs 4: Algorithms for Highly Efficient, Load-Balanced, and Scalable Molecular Simulation. J Chem Theory Comput. 2008; 4:435–447.
29. Hoover WG. Canonical Dynamics: Equilibrium Phase-Space Distributions. Phys Rev A. 1985; 31:1695–1697. [PubMed: 9895674]
30. Parrinello M, Rahman A. Polymorphic Transitions in Single-Crystals - a New Molecular-Dynamics Method. J Appl Phys. 1981; 52:7182–7190.
31. Jorgensen WL, Maxwell DS, TiradoRives J. Development and Testing of the Opls All-Atom Force Field on Conformational Energetics and Properties of Organic Liquids. J Am Chem Soc. 1996; 118:11225–11236.
32. Pasenkiewicz-Gierula M, Baczynski K, Murzyn K, Markiewicz M. Orientation of Lutein in a Lipid Bilayer - Revisited. Acta Biochim Pol. 2012; 59:115–118. [PubMed: 22428146]
33. Jorgensen WL, Chandrasekhar J, Madura JD, Impey RW, Klein ML. Comparison of Simple Potential Functions for Simulating Liquid Water. J Chem Phys. 1983; 79:926–935.
34. Hess B, Bekker H, Berendsen HJC, Fraaije JGEM. Lincs: A Linear Constraint Solver for Molecular Simulations. J Comp Chem. 1997; 18:1463–1472.
35. Essmann U, Perera L, Berkowitz ML, Darden T, Lee H, Pedersen LG. A Smooth Particle Mesh Ewald Method. J Chem Phys. 1995; 103:8577–8593.
36. Almeida PFF, Pokorny A, Hinderliter A. Thermodynamics of Membrane Domains. Biochim Biophys Acta Biomem. 2005; 1720:1–13.
37. Hyslop PA, Morel B, Sauerheber RD. Organization and Interaction of Cholesterol and Phosphatidylcholine in Model Bilayer-Membranes. Biochemistry. 1990; 29:1025–1038. [PubMed: 2160270]
38. Pasenkiewicz-Gierula M, Rog T, Kitamura K, Kusumi A. Cholesterol Effects on the Phosphatidylcholine Bilayer Polar Region: A Molecular Simulation Study. Biophys J. 2000; 78:1376–1389. [PubMed: 10692323]
39. Rog T, Pasenkiewicz-Gierula M. Cholesterol Effects on the Phosphatidylcholine Bilayer Nonpolar Region: A Molecular Simulation Study. Biophys J. 2001; 81:2190–2202. [PubMed: 11566790]

40. Edholm O, Nagle JF. Areas of Molecules in Membranes Consisting of Mixtures. Biophys J. 2005; 89:1827–1832. [PubMed: 15994905]
41. Smondyrev AM, Berkowitz ML. Molecular Dynamics Simulation of the Structure of Dimyristoylphosphatidylcholine Bilayers with Cholesterol, Ergosterol, and Lanosterol. Biophys J. 2001; 80:1649–1658. [PubMed: 11259280]
42. Seelig J, Seelig A. Lipid Conformation in Model Membranes and Biological Membranes. Q Rev Biophys. 1980; 13:19–61. [PubMed: 7220788]
43. Heller H, Schaefer M, Schulten K. Molecular-Dynamics Simulation of a Bilayer of 200 Lipids in the Gel and in the Liquid-Crystal Phases. J Phys Chem. 1993; 97:8343–8360.
44. Hubbell WL, McConnell HM. Molecular Motion in Spin-Labeled Phospholipids and Membranes. J Am Chem Soc. 1971; 93:314–26. [PubMed: 5541516]
45. Kneller GR, Baczynski K, Pasenkiewicz-Gierula M. Communication: Consistent Picture of Lateral Subdiffusion in Lipid Bilayers: Molecular Dynamics Simulation and Exact Results. J Chem Phys. 2011; 135:141105. [PubMed: 22010688]
46. Kinosita K, Kawato S, Ikegami A. Theory of Fluorescence Polarization Decay in Membranes. Biophys J. 1977; 20:289–305. [PubMed: 922121]
47. Kinosita K, Ikegami A, Kawato S. On the Wobbling-in-Cone Analysis of Fluorescence Anisotropy Decay. Biophys J. 1982; 37:461–464. [PubMed: 7059650]
48. Kusumi A, Pasenkiewiczgierula M. Rotational Diffusion of a Steroid Molecule in Phosphatidylcholine Membranes - Effects of Alkyl Chain-Length, Unsaturation, and Cholesterol as Studied by a Spin-Label Method. Biochemistry. 1988; 27:4407–4415. [PubMed: 3166984]
49. PasenkiewiczGierula M, Takaoka Y, Miyagawa H, Kitamura K, Kusumi A. Hydrogen Bonding of Water to Phosphatidylcholine in the Membrane as Studied by a Molecular Dynamics Simulation: Location, Geometry, and Lipid-Lipid Bridging Via Hydrogen-Bonded Water. J Phys Chem A. 1997; 101:3677–3691.
50. Rog T, Pasenkiewicz-Gierula M. Effects of Epicholesterol on the Phosphatidylcholine Bilayer: A Molecular Simulation Study. Biophys J. 2003; 84:1818–26. [PubMed: 12609883]
51. Huang J, Feigenson GW. A Microscopic Interaction Model of Maximum Solubility of Cholesterol in Lipid Bilayers. Biophys J. 1999; 76:2142–57. [PubMed: 10096908]
52. Huang J. Model Membrane Thermodynamics and Lateral Distribution of Cholesterol: From Experimental Data to Monte Carlo Simulation. Methods Enzymol. 2009; 455:329–64. [PubMed: 19289212]
53. Rog T, Pasenkiewicz-Gierula M, Vattulainen I, Karttunen M. What Happens If Cholesterol Is Made Smoother: Importance of Methyl Substituents in Cholesterol Ring Structure on Phosphatidylcholine-Sterol Interaction. Biophys J. 2007; 92:3346–57. [PubMed: 17293396]
54. Pandit SA, Bostick D, Berkowitz ML. Complexation of Phosphatidylcholine Lipids with Cholesterol. Biophys J. 2004; 86:1345–1356. [PubMed: 14990465]
55. Tu K, Klein ML, Tobias DJ. Constant-Pressure Molecular Dynamics Investigation of Cholesterol Effects in a Dipalmitoylphosphatidylcholine Bilayer. Biophys J. 1998; 75:2147–56. [PubMed: 9788908]
56. Chiu SW, Jakobsson E, Mashl RJ, Scott HL. Cholesterol-Induced Modifications in Lipid Bilayers: A Simulation Study. Biophys J. 2002; 83:1842–1853. [PubMed: 12324406]

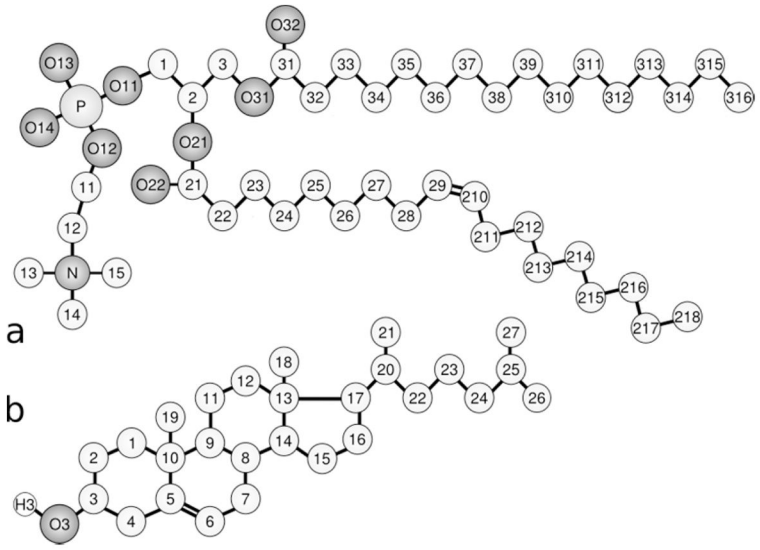


**Figure 1.**

Molecular structures of the POPC (a) and Chol (b) (POPC atoms are numbered according to Sundaralingam's nomenclature [27]—*2* signifies oleoyl and *3* the palmitoyl chain). In both structures, the chemical symbol for carbon atoms, C, and the hydrogen atoms are omitted, except for the Chol OH group, where the H atom is explicitly included.

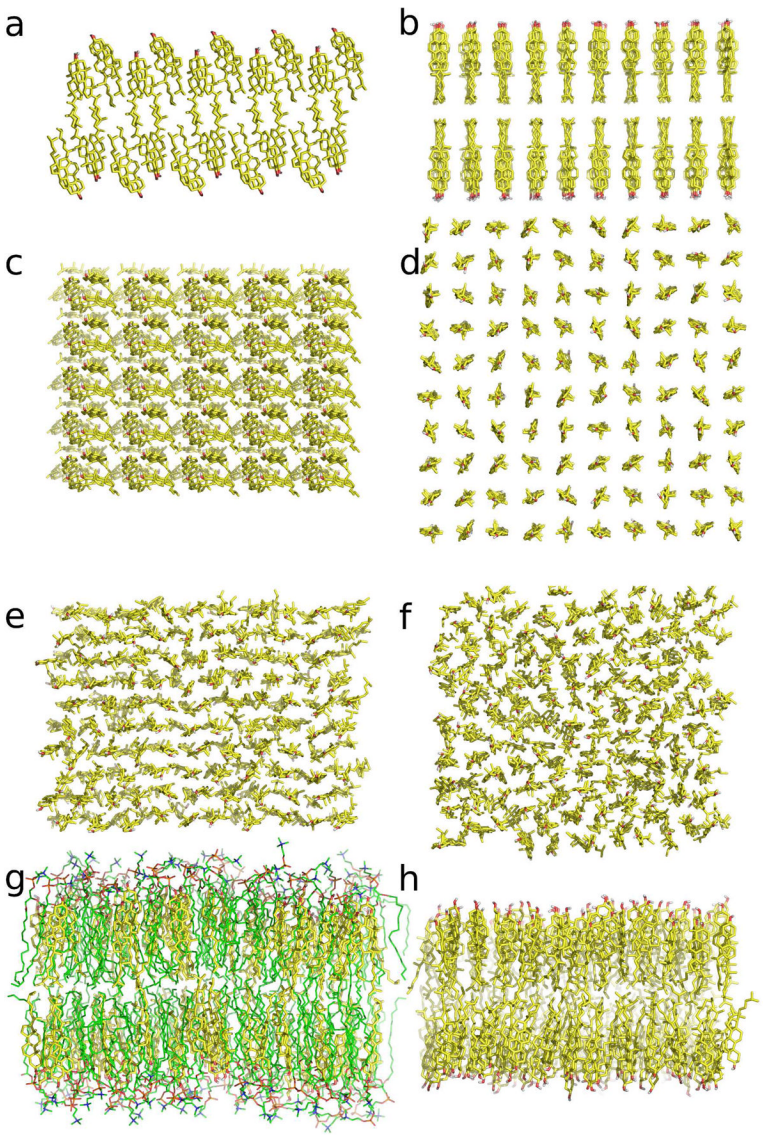


**Figure 2.**

Side (a) and top (c) views of the Chol crystal bilayer; side (b) and top (d) views of the initial structure of the Chol-2 bilayer; snapshots (top views) of the Chol (e) and Chol-2 (f) bilayers at the end of the respective MD trajectories (200 ns), and snapshots (side views) of the POPC-Chol50 (g) and Chol (h) bilayers at the end of the respective MD trajectories (200 ns). Water and hydrogen atoms are removed to better show the details of the bilayers. The Chol molecules are shown as yellow sticks. The OH group of Chol is shown in standard colors as the CPK model. The POPC atoms are coded in standard colors as lines.

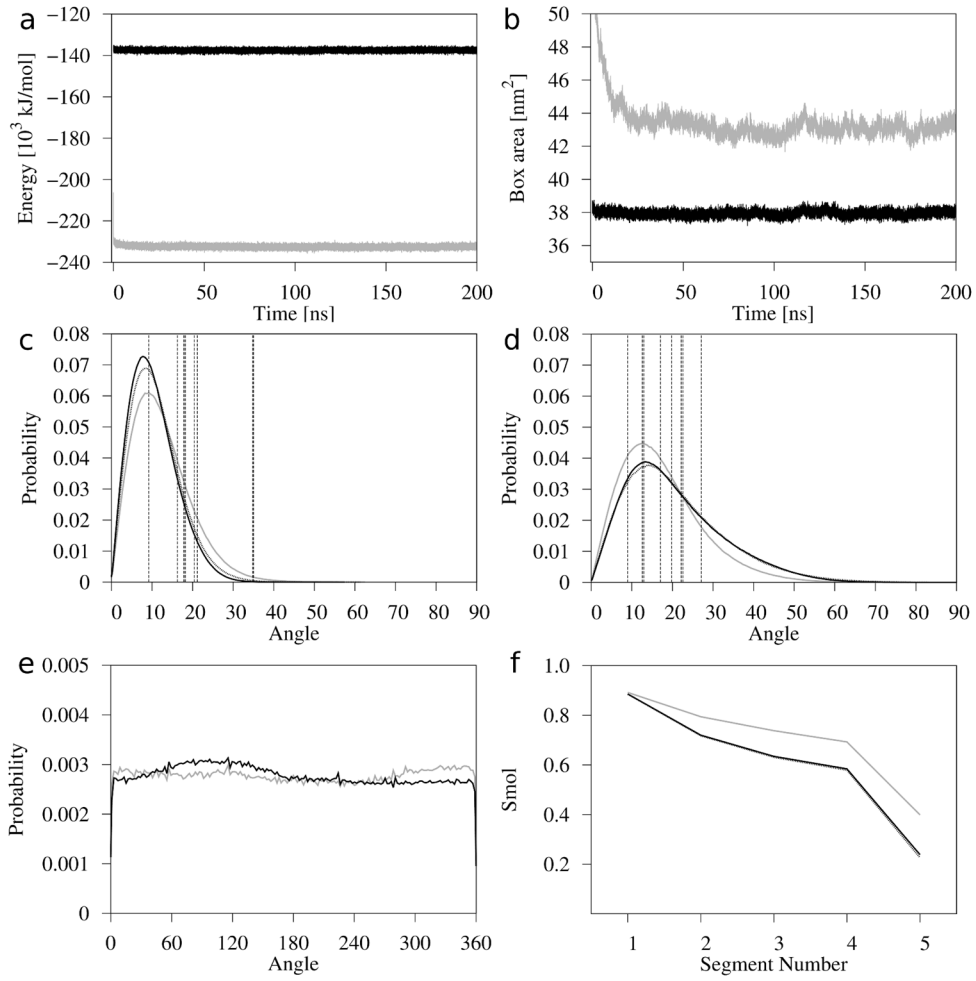


**Figure 3.**

Time profiles of the bilayer potential energy (a) and the simulation box surface area (b) along respective MD trajectories; distributions of tilt ($\theta$) angles for Chol rings (c) and chains (d); distribution of azimuthal ($\varphi$) angles for Chol rings (e); and the molecular order parameter ($S_{mol}$) profiles calculated for the Chol chains (f), for the Chol (black line), Chol-2 (black dotted line, c, d, and f), and POPC-Chol50 (gray line) bilayers. The vertical dashed lines in (c) and (d) represent tilts of the ring (c) and chain (d) of each of the eight Chol molecules in the unit cell of the anhydrous Chol crystal [20].

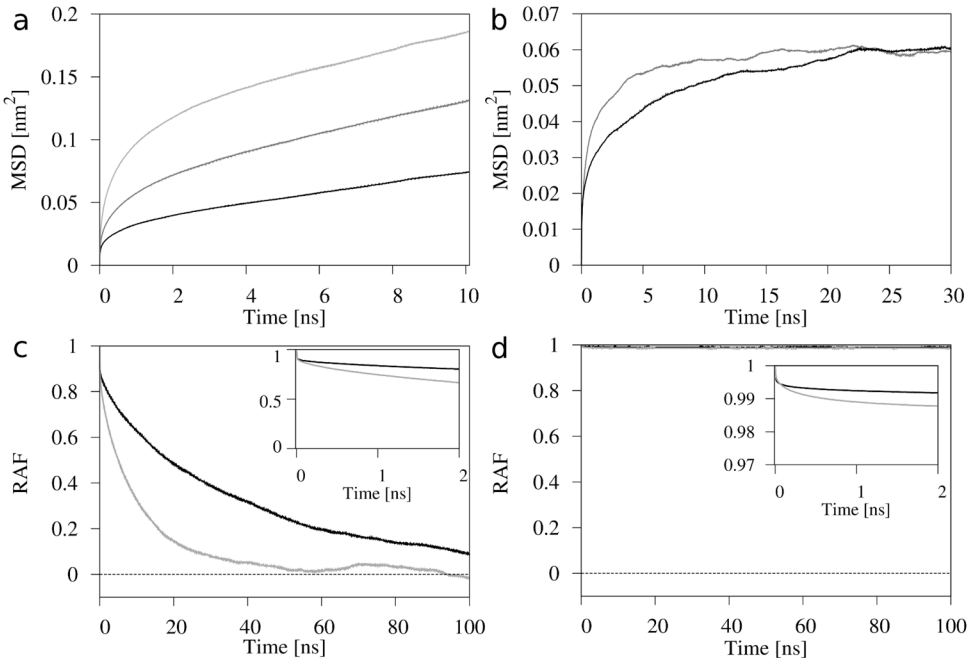


**Figure 4.**

Mean square displacement (MSD) curves for the lateral (a) and vertical (b) self-diffusion; and rotational autocorrelation functions (RAF) for the parallel (c) and perpendicular (d) rotation about and relative to the molecular axis, of Chol molecules in the Chol-2 (black line) and POPC-Chol50 (gray line) bilayers. In (a) and (b), motion of CMs of Chol molecules is calculated, and additionally in (a), the light gray curve is MSD for POPC molecules in the POPC-Chol50 bilayer. In (c) and (d), the insets show decays of the RAFs within first 2 ns.

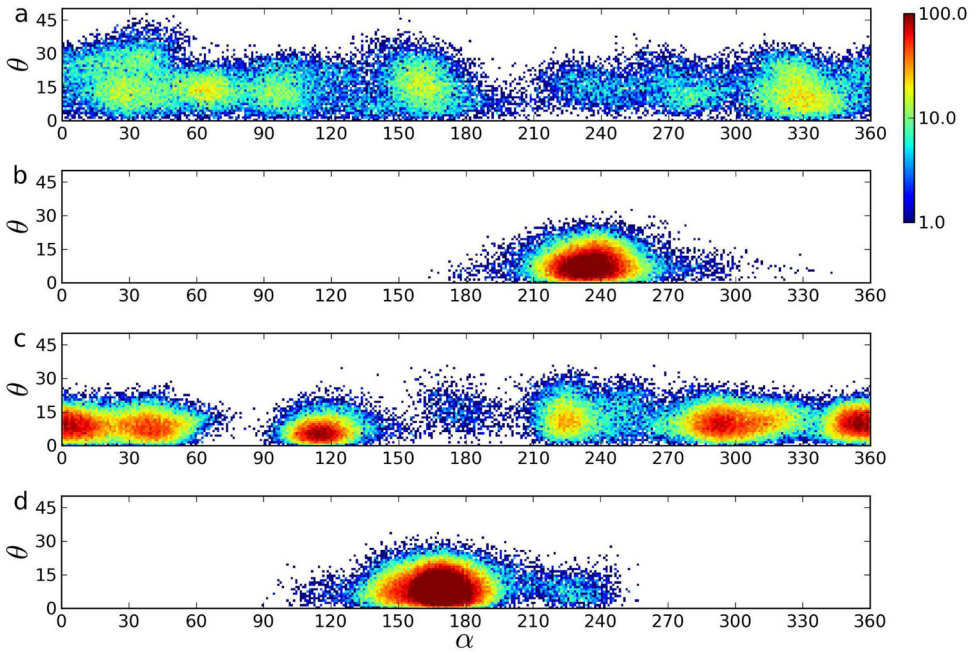


**Figure 5.**

Simultaneous populations of angles by Chol molecules rotating about their long axis ($\alpha$) and relative to the normal ($\theta$) during 100 ns sampled with a 1 ps time step for two representative Chol molecules in the POPC-Chol50 (a, b) and Chol-2 bilayers (c, d). The fastest rotating molecules about the long axis are represented in (a, c), and the slowest rotating molecules in (b, d). The angles $\alpha$ and $\theta$ are defined in the text. The color scale on the right-hand side codes logarithm of the number of cases when a given angle was populated during the analysis time. The white color indicates zero cases.

## Table 1

Average membrane parameters

| | Chol | 4Chol | PC-Chol50 | 4PC-Chol50 |
|---|---|---|---|---|
| Area (Å$^2$) | 38.0 ± 0.1<br>38.0 ± 0.2[b]<br>~37.0[c] | 37.9 ± 0.1 | 48.4 ± 0.5/PC[a]<br>38.0/Chol[d] | 48.4 ± 0.2/PC<br>38.0/Chol[d] |
| C-C dist. (Å) | 32.3 ± 2.6<br>32.3 ± 2.8[b]<br>30.5 ± 3.7[c] | 32.4 ± 2.8 | 34.4 ± 2.8 | 34.6 ± 2.9 |
| P-P dist. (Å) | | | 45.7 ± 2.7[a] | 45.7 ± 2.9 |
| $S_{mol}$ | 0.61 ± 0.01<br>0.61 ± 0.01[b] | 0.61± 0.01 | 0.70 ± 0.01 | 0.69±0.01 |
| Tilt (°) | | | | |
| C3-C17 | 8.0; (10.7 ± 5.8) 8.3[b]; (11.0± 6.1)[b] | 7.8 (10.4 ± 5.6) | 9.1 (12.3 ± 6.9) | 9.3 (12.5 ± 7.1) |
| C17-C25 | 13.4; (20.9 ± 12.5) 12.8[b]; (20.8 ± 12.7)[b] | 13.3 (20.4 ± 11.8) | 12.6 (17.3 ± 10.1) | 12.3 (17.3 ± 10.0) |
| #H-bonds/Chol | 2.29 ± 0.05<br>2.29 ± 0.05[b] | 2.29 ± 0.03 | 1.68 ± 0.08 | 1.70 ± 0.04 |
| MSD(10 ns) (Å$^2$) | 5.92 ± 1.2<br>7.37 ± 3.3[b] | 5.95± 2.7 | 13.0 ± 4.8/Chol<br>18.5 ± 5.0/PC | 13.4 ± 4.3/Chol<br>20.0 ± 4.8/PC |

Average values of the surface area available to the lipid (Area); distance between average positions of carbon C3 or phosphorus P atoms in the two leaflets of a bilayer (C-C dist.; P-P dist.); molecular order parameter, Smol, for the cholesterol hydrocarbon chains; tilt angle (Tilt) of the cholesterol rings (C3-C17) and chains (C17-C25); and number of Chol-water H-bonds per Chol (#H-bond/Chol); together with values of mean square displacement after 10 ns (MSD), in the Chol (Chol-2), and POPC-Chol50 bilayers as well as in the 4Chol and 4POPC-Chol50 bilayers. The errors are standard deviation estimates, except for Smol, where they are standard error estimates. For tilt, the most probable, and, in parentheses, the average and standard deviation values are given. For comparison, some values for the Chol crystal bilayers are also given.

[a] From Ref. 19

[b] Chol-2 bilayer

[c] Chol crystal bilayer (anhydrous crystal)[20]

[d] The value of $A_{Chol}$ was fixed to the value obtained from the pure Chol bilayers